Micromachining

DOI: 10.1002/anie.201204600

Enzymatic Sculpting of Nanoscale and Microscale Surface Topographies**

*Jen-Huang Huang, Arul Jayaraman, and Victor M. Ugaz**

Living systems display complex structured nano- and microscale topologies that orchestrate a host of physical and biological functions.[1] But these features can be challenging to replicate using conventional planar methods,[2] and nanometer-scale structures cannot be readily constructed without dedicated facilities.[3] Herein we show how enzymatic activity can be harnessed to fashion complex nano- and microscale surface topographies on biodegradable substrates. Coordinated patterning and machining are accomplished by manipulating interactions between an enzyme, substrate, and protein inhibitor. In this way, we are able to construct nanochannels, microchannels containing embedded features templated by the substrate's crystalline morphology, and a membraneless filter capable of isolating rare cells from whole blood with a throughput that is orders of magnitude greater than currently possible. In addition to enabling molecularly imprinted surface landscapes mimicking those in living systems to be fashioned by a straightforward process accessible in virtually any laboratory, considerable potential exists to exquisitely control the underlying biochemical interactions by employing enzymes and substrates with appropriately engineered properties.

Our bioinspired machining approach exploits the enzymatic activity of proteinase K (PK), a serine protease capable of cleaving peptide bonds with particular affinity toward alanine–alanine linkages.[4] Poly(lactic acid) (PLA) serves as a convenient substrate because it is also susceptible to this degradation mechanism owing to structural similarities between lactic acid and alanine. Machining is initiated when PK is transported from the bulk environment to the PLA surface, after which enzyme–substrate complexation catalyzes surface reactions yielding low-molecular-weight cleavage products that subsequently become hydrolyzed and are released into the bulk along with dissociated PK (Figure 1 a). Patterned machining is accomplished by directing an aqueous PK solution through a microfluidic template (constructed from poly(dimethyl siloxane), PDMS) using conventional soft

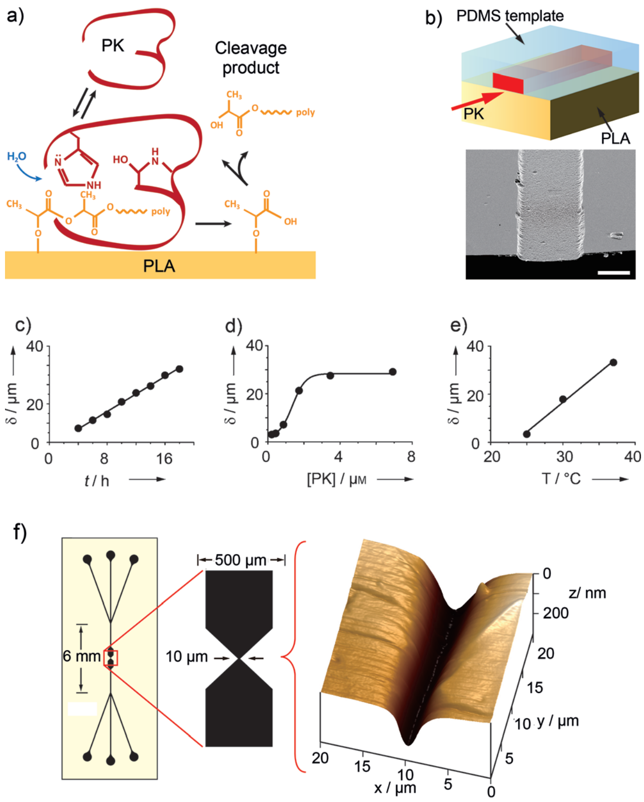

Figure 1. Enzymatic nano- and micromachining. a) Biochemical degradation cycle between proteinase K (PK) and the PLA substrate. b) Cross-sectional view (left) illustrating how machining is performed by directing an aqueous PK solution through a PDMS microchannel template bonded to a PLA sheet. Scale bar in SEM image (right): 200 μm. c) Feature depth *d* versus time ([PK] = 6.92 μM (0.2 $mg\,mL^{-1}$), 5 $\mu L\,min^{-1}$, 37 °C). d) Depth versus enzyme concentration (5 $\mu L\,min^{-1}$, 37 °C, 16 h). e) Depth versus temperature ([PK] = 6.92 μM, 5 $\mu L\,min^{-1}$, 16 h). f) A nanochannel (170 nm deep) is constructed by injecting PK into a PDMS template (left) for 3 h at 25 °C. Machining is laterally confined within a circa 4 μm-wide zone by hydrodynamic focusing of PK between co-injected streams of bovine serum albumin (2 $\mu L\,min^{-1}$ each stream; see also Figure 2). The *z*-axis of the AFM profile (right) is expanded to show detail.

lithography so that the ensuing enzymatic degradation imprints a replica of the flow path into a PLA substrate on the microchannel floor (Figure 1 b). Characteristic degradation rates of 2 $\mu m\,h^{-1}$ are achievable in a 300 μm-wide, 10.7 mm-long microchannel (Figure 1 c). Feature depths increase monotonically with enzyme concentration up to about 4 μM, above which surface complexation sites become saturated (Figure 1 d).[5] Machining also reflects temperature-dependent enzymatic activity, which occurs about 7 times

[*] J.-H. Huang, Prof. A. Jayaraman, Prof. V. M. Ugaz
Artie McFerrin Department of Chemical Engineering
Texas A&M University, 3122 TAMU
College Station, TX 77843 (USA)
E-mail: ugaz@tamu.edu

[**] This work was supported in part by the US National Science Foundation under grant DMR-1106005 monitored by Dr. Joseph Akkara. J.-H.H. acknowledges support from a Texas A&M University Dissertation Fellowship. We thank Dr. Jeongyun Kim and Dr. Maria King for assistance with cell separation experiments, and Mr. Aashish Priye for helpful discussions about the flow network design.

Supporting information for this article is available on the WWW under http://dx.doi.org/10.1002/anie.201204600.

faster at 37 °C than at room temperature (Figure 1 e). These rates enable nanometer-size features to be easily imprinted, as illustrated by construction of a 170 nm-deep channel by injection of a PK solution at 2 μL min^{-1} for 3 h at room temperature (Figure 1 f).

There is a critical need for methods that can enable rapid and continuous harvesting of cells and cell-sized components from blood, but current technologies often require timescales of hours (and sometimes tens of hours) to process standard 5 mL samples.[6] Enzymatic micromachining has enabled us to develop a new approach that overcomes these limitations because it operates most efficiently at high flow rates. This filtration architecture is fashioned by co-injecting a 1 % w/v aqueous solution containing bovine serum albumin (BSA) to spatially regulate the etching process (Figure 2 a). Complexation between proteinase K and the BSA protein establishes a competitive interaction that inactivates the laterally diffusing enzyme before it can attack the PLA substrate so that the boundary of the etched region can be sharply defined. The size of the etched zone can be manipulated by adjusting the BSA concentration to vary the driving force for lateral diffusion with respect to the adjoining PK. This mechanism can be exploited to construct microchannels incorporating weir-like barriers oriented parallel to the flow direction by sequentially varying the composition in each stream (Figure 2 b). First, BSA solution is injected into the center steam while PK is introduced into both outer streams, thereby etching the PLA substrate to a depth of 10 μm on either side of the central zone protected from enzymatic degradation by the BSA. Next, BSA is infused into both the center stream and one of the outer streams; thereafter etching is continued, yielding different depths on each side of the microchannel. Finally, PK is injected into all three inlets to define the height of the centerline barrier (Figure 2 c); this topology is preserved along the entire length of the microchannel (Supporting Information, Figure S1a). Feature sizes can be further tuned by varying the relative flow rates of BSA and PK to hydrodynamically focus the desired streams (Supporting Information, Figure S1b). The machined structures can be used as-is, or alternatively the rigid PLA substrate can serve as a re-usable master mold for replication in PDMS by soft lithography (Supporting Information, Figure S2). Thus, even though micrometer-scale enzymatic machining may be relatively slow, the resulting structures are amenable for mass production.

This arrangement, coupled with the secondary transverse motion generated within the curved flow path,[7] creates a driving force that transports smaller-sized components across the barrier from the inner lane to the outer lane while larger-sized species are retained in the inner lane. Further enrichment occurs owing to unequal depths on each side of the weir (Figure 3 a). To demonstrate practical application, we next used this filtration device to harvest PC3 human prostate cancer cells (20–30 μm diameter) from whole blood (injected component densities: PC3 1.43×10^6 cells mL^{-1}, WBC 1.22×10^6 cells mL^{-1}, RBC 7.32×10^8 cells mL^{-1}). The PC3-spiked blood sample was injected into the inner lane at 1 mL min^{-1} (PBS was co-injected into the outer lane at the same flow rate). Cell counts indicate that PC3 cells were harvested with more than 99 % efficiency (Figure 3 b) and 1.6-fold enrichment

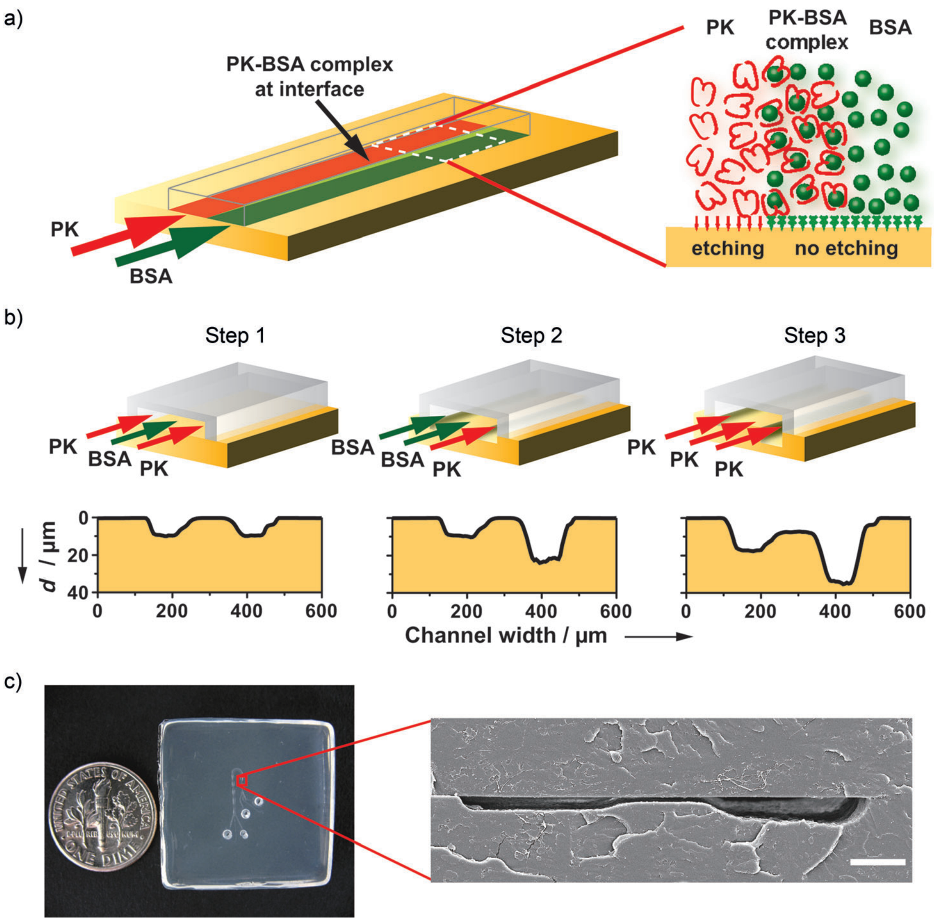

Figure 2. Machining is governed by a competitive interaction between enzyme, substrate, and inhibitor. a) When PK (etchant, red) and BSA (inhibitor, green) are co-injected into a Y-shaped microchannel, a localized interfacial zone of PK-BSA complexation establishes the boundary of the etched region. b) Alternating flows of PK and BSA are introduced to fashion a microchannel, the depth *d* of which varies along the cross-section. Surface profiles are obtained 0.5 cm from the inlet ([PK] = 6.92 μM, [BSA] = 1 % w/v (150.6 μM), all flow rates = 5 μL min^{-1}). c) Top-view photograph of the assembled filtration device (left) and SEM image of enzymatically machined microchannel cross-section (right; bar, 50 μm).

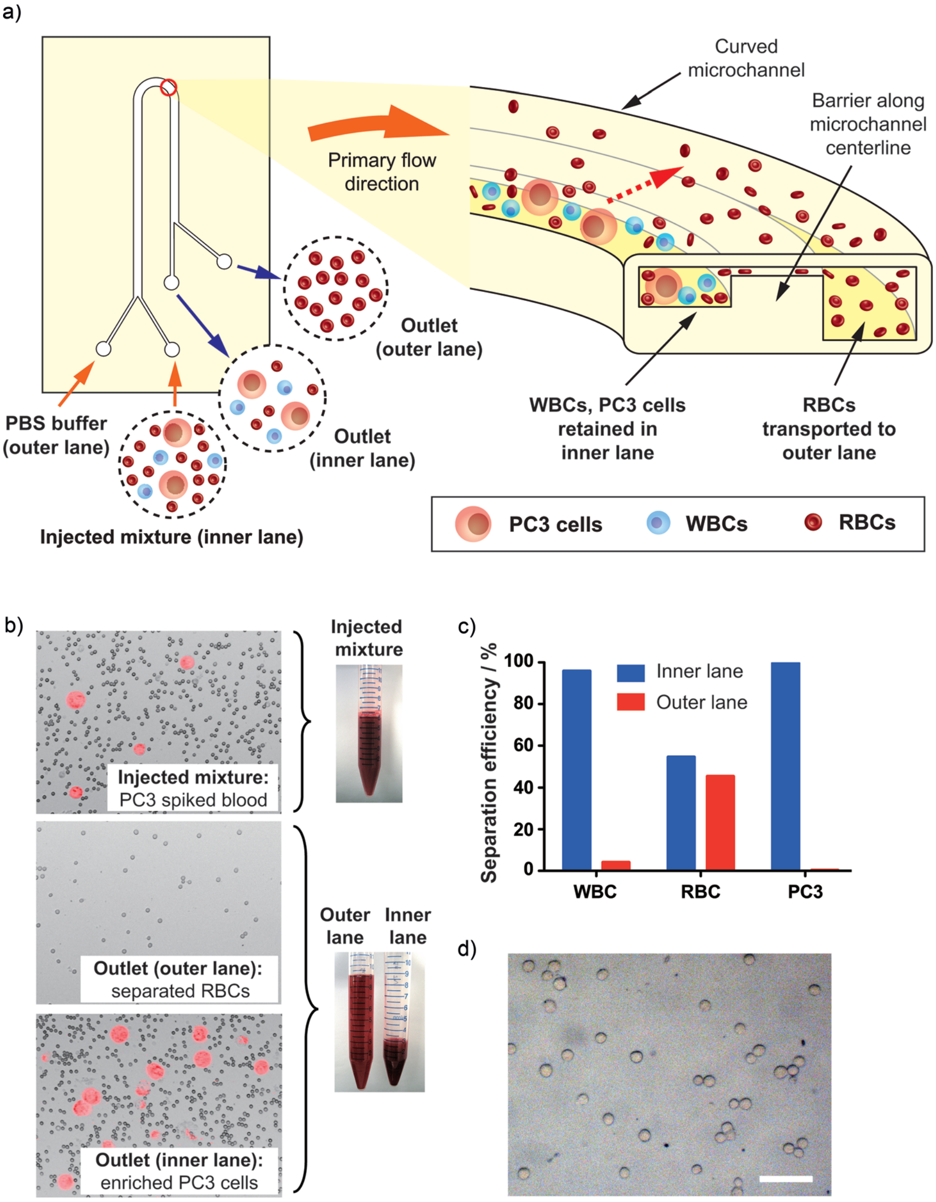

Figure 3. An enzymatically machined membraneless architecture enables high-throughput cell harvesting. a) Illustration and cross-sectional profile (inner and outer lanes: 20 and 35 μm deep, respectively, centerline barrier gap: 3 μm deep, radius of curvature: 500 μm). b) Separation of whole blood spiked with PC3 cancer cells at 1 mL min^{-1}, showing isolation and enrichment of PC3 cells from whole blood (inner lane). c) Cell-count data show the relative fractions of WBCs, RBCs, and PC3 cells recovered at the inner lane. d) Viability of PC3 cells is unchanged after filtration (trypan blue assay, viable cells unstained; bar, 50 μm).

upon recovery from the inner lane (45 % of RBCs, 4 % of WBCs, and less than 1 % of PC3 cells cross to the outer lane). The enriched cells were maintained in the as-injected blood environment with no discernible change in viability (before filtration: $98.7\pm0.6\,\%$, $n=3$; after filtration: $98.9\pm0.1\,\%$, $n=3$; Figure 3c).

A key benefit of our approach is the capability for high-throughput operation, and this can be seen upon comparison with existing methods for isolation of rare-cell biomarkers relevant to cancer (for example, circulating tumor cells (CTCs); Table 1; results are expressed in terms of normalized throughput representing the time to process 1 mL of undiluted whole blood). Not only is our approach orders of magnitude faster than comparable methods, it also delivers $99.2\pm0.2\,\%$ ($n=3$) retention of PC3 cells from spiked whole blood and $99.7\pm0.5\,\%$ ($n=3$) when dispersed in PBS buffer. No additional steps are required to retrieve the separated cells, in contrast to conventional membrane or affinity capture approaches. These advantages suggest considerable untapped potential to enable a wide range of blood-cell analysis applications where harvesting throughput is currently a limiting constraint (for example, granulocyte isolation,[6b,8] cancer-cell analysis[9]).

In the context of CTC analysis, we remark that immunoselection (the current gold standard) requires pre-programming with antibodies to enable recognition of specific epithelial antigens expressed by CTCs, thus limiting the ability to capture different cell types and introducing the possibility of retaining non-malignant cells. Optimal capture efficiencies are achieved by applying low flow rates and increasing the binding surface area (requiring more antibodies), with additional wash steps and reagents necessary to recover the captured cells. CTCs have also been efficiently separated by dielectrophoresis, but the cells must be dispersed in isotonic buffers at high dilution, and low flow rates are required. Physical barrier filtration architectures also achieve high separation efficiency, but high dilution and low flow rates are needed to prevent clogging. Methods exploiting other hydrodynamic effects also generally require high dilution and often operate within a narrow "sweet spot" of cell size and flow rate. Our approach overcomes these throughput limitations because separation occurs optimally at high flow rates, with considerable potential for further improvement by employing multistaged designs that sequentially feed the enriched effluent into additional downstream filtration elements. Multiple weirs with different widths, depths, and gaps can also be arrayed in parallel to process multicomponent mixtures.

Table 1: Comparison of microfluidic-based CTC enrichment methods.

Method	Flow rate (reported)	Dilution factor	Normalized throughput[a] [$mL\,min^{-1}$]	CTC recovery	Ref.	Comments
This work	**1 $mL\,min^{-1}$**	**5**	**0.2**	**99%**		**· Optimal operation at high flow rates**
Immunoselection (bead-based)	10 $mL\,h^{-1}$	>1[b]	unknown[b]	90%	[10]	· Antibody-based
	240 $\mu L\,min^{-1}$	>1[b]	unknown[b]	85%	[11]	· Additional washing
Immunoselection (micropost array)	1 $mL\,h^{-1}$	1	0.017	65–80%	[9]	· Antibody-based · Low volume capacity
	1 $mL\,h^{-1}$	1	0.017	95%	[12]	
	2 $mL\,h^{-1}$	1	0.03	92%	[13]	
Dielectrophoresis	1.5 $ml\,min^{-1}$	40000	3.75×10^{-5}	90%	[14]	· Special buffer conditions
	126 $\mu L\,min^{-1}$	400	3.15×10^{-4}	75%	[15]	
Physical barrier						· Dilution and/or low flow rate operation needed to avoid clogging
· Pool-dam	0.1 $mL\,min^{-1}$	5000	2×10^{-5}	99%	[16]	
· Isolation wells	0.7 $mL\,h^{-1}$	3	3.9×10^{-3}	80%	[17]	
Hydrodynamics						· Dilution and/or low flow rate operation needed to avoid clogging
· Expansion/contraction	0.4 $mL\,min^{-1}$	20	0.02	80%	[18]	
· Microvortex trapping	4.5 $mL\,min^{-1}$	40	0.11	85%	[19]	

[a] The time to process 1 mL of undiluted whole blood. [b] Normalized throughput was difficult to assess owing to the incubation, washing, and resuspension steps inherent to bead-based capture methods.

The highly specific nature of enzyme–substrate interactions can also be exploited to enable direct imprinting of molecular-scale topologies. We explored this potential by taking advantage of the machining rate selectivity to PLA crystallinity (increasing the degree of crystallinity from 0 to 50% yields a ten-fold decrease in the material degradation rate[20]) to embed morphological features associated with the crystalline domains of the substrate within a fluidic channel (Figure 4a). The crystalline morphology is in turn governed by thermal history (annealing time and temperature, cooling rate) and material properties (molecular weight, stereoisomers and their blends), thus permitting broad control over the imprinted topologies (Supporting Information, Figure S3). Machining after the PLA is continuously cooled from the melt exposes a dendritic surface topology (Figure 4b), whereas an array of obstacles reflecting the size and density of spherulitic crystalline domains emerges when PK is injected following a low-temperature anneal (70°C for 8 h; Figure 4c). By controlling annealing time and temperature, the extent and distribution of crystallinity within the substrate can be manipulated[21] to enable post-like arrays with tunable size and density to be embedded within a micro- or nanoscale fluidic channel in a lithography-free manner (for example, as barrier or packing structures for filtration and chromatography).

Enzymatic machining introduces an unexplored avenue to fashion molecularly imprinted surface features by a simple process that can be accessed in virtually any laboratory. More broadly, the highly specific nature of the governing interactions lays a foundation to exquisitely control the templated nanoscale morphologies by manipulating properties of the enzyme and substrate. For example, various classes of biodegradable polymers are selectively machined by different enzymes (for example, polycaprolactone (PCL) can be degraded by lipase,[22] and numerous strains of the bacterial classes *Firmicutes* and *Proteobacteria* can degrade PCL, polyhydroxybutyrate, and polybutylene succinate[23]). These interactions can be further tuned by engineering enzymes displaying enhanced activities and specificities that can be toggled in response to environmental cues, as well as by employing substrates containing assembled crystalline morphologies.

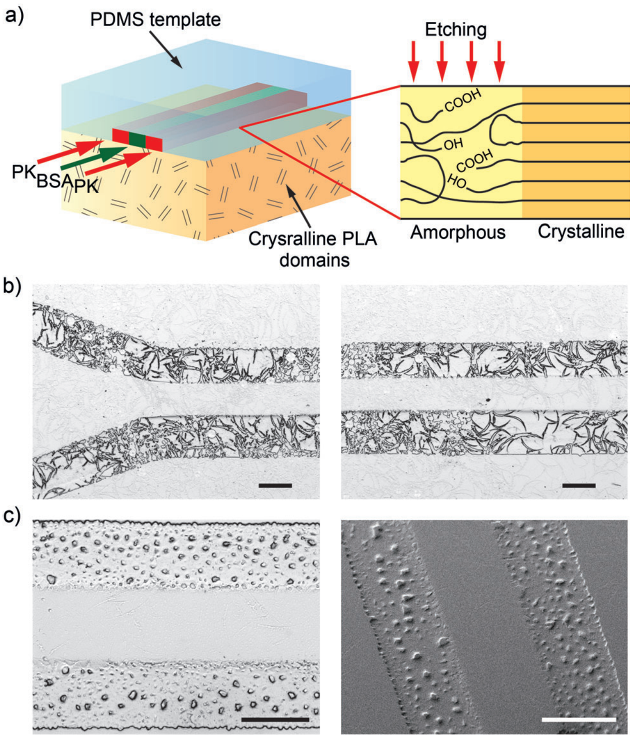

Figure 4. Machining molecularly templated surface topographies. a) Morphologically governed selectivity is made possible by differences in the rate of PK-mediated degradation between hydrolysis-resistant crystalline domains and amorphous regions containing condensed hydrophilic and catalytic terminal groups (OH and COOH). b) Machining after continuous slow cooling from 180°C exposes dendritic features. c) Machining after annealing at 70°C for 8 h embeds an array of post-like obstacles within the microchannel (a 3D topology is evident in the SEM image, right). PK was injected at 37°C for 2 h. Scale bars: 100 μm.

Received: June 13, 2012
Published online: August 24, 2012

Keywords: biomaterials · enzymes · microfluidics · nanofabrication · patterning

[1] a) A. S. Crouch, D. Miller, K. J. Luebke, W. Hu, *Biomaterials* **2009**, *30*, 1560–1567; b) M. Khabiry, B. G. Chung, M. J. Hancock, H. C. Soundararajan, Y. N. Du, D. Cropek, W. G. Lee, A. Khademhosseini, *Small* **2009**, *5*, 1186–1194; c) A. T. O'Neill, N. A. Monteiro-Riviere, G. M. Walker, *Lab Chip* **2009**, *9*, 1756–1762; d) X. F. Walboomers, J. A. Jansen, *Odontology* **2001**, *89*, 2–11; e) X. Y. Zhu, K. L. Mills, P. R. Peters, J. H. Bahng, E. H. Liu, J. Shim, K. Naruse, M. E. Csete, M. D. Thouless, S. Takayama, *Nat. Mater.* **2005**, *4*, 403–406.

[2] A. M. Taylor, M. Blurton-Jones, S. W. Rhee, D. H. Cribbs, C. W. Cotman, N. L. Jeon, *Nat. Methods* **2005**, *2*, 599–605.

[3] a) L. J. Guo, X. Cheng, C. F. Chou, *Nano Lett.* **2004**, *4*, 69–73; b) J. Li, D. Stein, C. McMullan, D. Branton, M. J. Aziz, J. A. Golovchenko, *Nature* **2001**, *412*, 166–169; c) J. M. Perry, K. Zhou, Z. D. Harms, S. C. Jacobson, *ACS Nano* **2010**, *4*, 3897–3902; d) S. M. Stavis, E. A. Strychalski, M. Gaitan, *Nanotechnology* **2009**, *20*, 165302; e) J. D. Uram, K. Ke, A. J. Hunt, M. Mayer, *Angew. Chem.* **2006**, *118*, 2339–2343; *Angew. Chem. Int. Ed.* **2006**, *45*, 2281–2285.

[4] W. Ebeling, N. Hennrich, M. Klockow, H. Metz, H. D. Orth, H. Lang, *Eur. J. Biochem.* **1974**, *47*, 91–97.

[5] a) A. Göopferich, R. Langer, *Macromolecules* **1993**, *26*, 4105–4112; b) A. Göpferich, *Biomaterials* **1996**, *17*, 103–114; c) S. Roy, J. M. Thomas, E. A. Holmes, J. T. Kellis, Jr., A. J. Poulose, C. R. Robertson, A. P. Gast, *Anal. Chem.* **2005**, *77*, 8146–8150.

[6] a) M. Cristofanilli, G. T. Budd, M. J. Ellis, A. Stopeck, J. Matera, M. C. Miller, J. M. Reuben, G. V. Doyle, W. J. Allard, L. W. M. M. Terstappen, D. F. Hayes, *New Engl. J. Med.* **2004**, *351*, 781–791; b) A. Mantovani, M. A. Cassatella, C. Costantini, S. Jaillon, *Nat. Rev. Immunol.* **2011**, *11*, 519–531.

[7] A. P. Sudarsan, V. M. Ugaz, *Proc. Natl. Acad. Sci. USA* **2006**, *103*, 7228–7233.

[8] K. T. Kotz, W. Xiao, C. Miller-Graziano, W. J. Qian, A. Russom, E. A. Warner, L. L. Moldawer, A. De, P. E. Bankey, B. O. Petritis, D. G. Camp, A. E. Rosenbach, J. Goverman, S. P. Fagan, B. H. Brownstein, D. Irimia, W. H. Xu, J. Wilhelmy, M. N. Mindrinos, R. D. Smith, R. W. Davis, R. G. Tompkins, M. Toner, I. H. R. Injury, *Nat. Med.* **2010**, *16*, 1042–1047.

[9] S. Nagrath, L. V. Sequist, S. Maheswaran, D. W. Bell, D. Irimia, L. Ulkus, M. R. Smith, E. L. Kwak, S. Digumarthy, A. Muzikansky, P. Ryan, U. J. Balis, R. G. Tompkins, D. A. Haber, M. Toner, *Nature* **2007**, *450*, 1235–1239.

[10] K. Hoshino, Y. Y. Huang, N. Lane, M. Huebschman, J. W. Uhr, E. P. Frenkel, X. Zhang, *Lab Chip* **2011**, *11*, 3449–3457.

[11] B. D. Plouffe, M. Mahalanabis, L. H. Lewis, C. M. Klapperich, S. K. Murthy, *Anal. Chem.* **2012**, *84*, 1336–1344.

[12] S. T. Wang, K. Liu, J. A. Liu, Z. T. F. Yu, X. W. Xu, L. B. Zhao, T. Lee, E. K. Lee, J. Reiss, Y. K. Lee, L. W. K. Chung, J. T. Huang, M. Rettig, D. Seligson, K. N. Duraiswamy, C. K. F. Shen, H. R. Tseng, *Angew. Chem.* **2011**, *123*, 3140–3144; *Angew. Chem. Int. Ed.* **2011**, *50*, 3084–3088.

[13] S. L. Stott, C. H. Hsu, D. I. Tsukrov, M. Yu, D. T. Miyamoto, B. A. Waltman, S. M. Rothenberg, A. M. Shah, M. E. Smas, G. K. Korir, F. P. Floyd, Jr., A. J. Gilman, J. B. Lord, D. Winokur, S. Springer, D. Irimia, S. Nagrath, L. V. Sequist, R. J. Lee, K. J. Isselbacher, S. Maheswaran, D. A. Haber, M. Toner, *Proc. Natl. Acad. Sci. USA* **2010**, *107*, 18392–18397.

[14] P. R. C. Gascoyne, J. Noshari, T. J. Anderson, F. F. Becker, *Electrophoresis* **2009**, *30*, 1388–1398.

[15] H. S. Moon, K. Kwon, S. I. Kim, H. Han, J. Sohn, S. Lee, H. I. Jung, *Lab Chip* **2011**, *11*, 1118–1125.

[16] Z. Z. Chen, S. Y. Zhang, Z. M. Tang, P. F. Xiao, X. Y. Guo, Z. H. Lu, *Surf. Interface Anal.* **2006**, *38*, 996–1003.

[17] S. J. Tan, L. Yobas, G. Y. H. Lee, C. N. Ong, C. T. Lim, *Biomed. Microdevices* **2009**, *11*, 883–892.

[18] A. A. Bhagat, H. W. Hou, L. D. Li, C. T. Lim, J. Han, *Lab Chip* **2011**, *11*, 1870–1878.

[19] S. C. Hur, A. J. Mach, D. Di Carlo, *Biomicrofluidics* **2011**, *5*, 022206.

[20] R. T. MacDonald, S. P. McCarthy, R. A. Gross, *Macromolecules* **1996**, *29*, 7356–7361.

[21] S. D. Park, M. Todo, K. Arakawa, *J. Mater. Sci.* **2005**, *40*, 1055–1058.

[22] Y. Tokiwa, T. Suzuki, *Nature* **1977**, *270*, 76–78.

[23] T. Suyama, Y. Tokiwa, P. Ouichanpagdee, T. Kanagawa, Y. Kamagata, *Appl. Environ. Microbiol.* **1998**, *64*, 5008–5011.